IEEE Access
Multidisciplinary | Rapid Review | Open Access Journal

Received October 22, 2020, accepted November 1, 2020, date of publication November 5, 2020, date of current version November 18, 2020.

Digital Object Identifier 10.1109/ACCESS.2020.3036167

Accurate Fault Location Method of the Mechanical Transmission System of Shearer Ranging Arm

QINGHUA MAO[1,2], YONGQIANG ZHANG[1,2], XUHUI ZHANG[1,2], (Member, IEEE), GUANGMING ZHANG[3], HONGWEI FAN[1,2], AND KUNDAYI MUSHAYI[1,2]

[1]School of Mechanical Engineering, Xi'an University of Science and Technology, Xi'an 710054, China
[2]Shaanxi Key Laboratory of Mine Electromechanical Equipment Intelligent Monitoring, Xi'an University of Science and Technology, Xi'an 710054, China
[3]Faculty of Engineering and Technology, General Engineering Research Institute, Liverpool John Moores University, Liverpool L35UX, U.K.

Corresponding author: Qinghua Mao (maoqh@xust.edu.cn)

This work was supported in part by the National Natural Science Foundation of China under Grant 51875451 Grant 51974228, and Grant 61674121, in part by the Shaanxi Province Key Research and Development Project under Grant 2019GY-09 and Grant 2018TD-ZDCXL-GY-06-04, in part by the Shaanxi Coal Joint Fund with Shaanxi Provincial Department of Science and Technology under Grant 2019JLM-39, and in part by the Shaanxi Province Innovative Talents Project under Grant 2018TD-032. The work of Qinghua Mao was supported by the Chinese Scholarship Council, U.K.

ABSTRACT In the process of coal mine production, the fault of the mechanical transmission system of the shearer ranging arm directly affects safety production. Therefore, it is very important to achieve the accurate fault location of the shearer ranging arm. The combination method of optimized continuous complex Morlet wavelet envelope demodulation spectrum analysis and spectrum analysis is proposed. Firstly, the spectrum contrast analysis of vibration signals between the normal state and fault state is performed, which can obtain the fault characteristics frequency and preliminary fault location. Then, the optimized continuous complex Morlet wavelet envelope demodulation algorithm is proposed to extract the side-bands characteristics of vibration signals, which can obtain the rotation frequency of fault location by the contrast analysis of side-bands characteristics in normal and fault state. In the algorithm, the center frequency and bandwidth of Morlet wavelet are optimized by wavelet Shannon entropy, and the optimal scale factor can be accurately determined by spectrum contrast analysis of vibration signals in normal and fault state. Finally, the accurate gear fault location is achieved by comprehensive analysis results of optimized continuous complex Morlet wavelet envelope demodulation spectrum and spectrum contrast. The simulation signals and practical vibration signals are applied to verify the proposed accurate gear fault location method. The experiment results indicate that the center frequency and bandwidth determined by wavelet Shannon entropy make the wavelet waveform best match the fault impact signal, and the optimal scale factor can be accurately determined by spectrum contrast analysis of vibration signals in normal and fault state, and the proposed method can achieve the precise fault location of the mechanical transmission system of shearer ranging arm. It provides the method for the on-site rapid accurate fault location of the mechanical transmission system. It is of great significance to the safe and efficient production of the coal mine.

INDEX TERMS Shearer, mechanical transmission system, fault, envelope demodulation.

I. INTRODUCTION

The shearer is the key equipment of modern fully mechanized mining face, which is used in harsh environment. It easily subjects to large impact load from hard coals and rocks, and corrosion from water vapor and coal dust during operation. Also, it is improperly managed, operated, and maintained by workers. For these reasons, the failures frequently caused in the mechanical transmission system of the shearer ranging arm. The failures will lead to equipment damage and production interruption, great economic losses, and even casualties. Due to the complicated working conditions, long transmission chain and complicated structure, the fault diagnosis of mechanical transmission system of shearer ranging arm is still difficult. Both the gear and bearing fault of the shearer ranging arm will appear. However, the main fault is the gear fault,which is presented in Figure 1. Therefore, the gear fault diagnosis is deeply studied in this article.

The associate editor coordinating the review of this manuscript and approving it for publication was Vicente Alarcon-Aquino.

This work is licensed under a Creative Commons Attribution 4.0 License. For more information, see https://creativecommons.org/licenses/by/4.0/

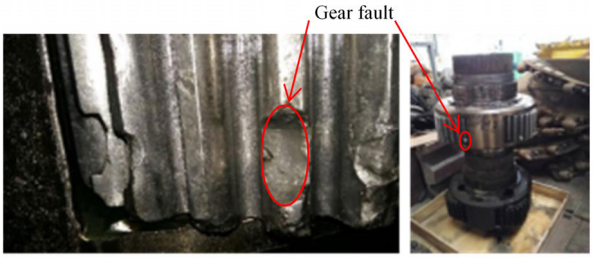

FIGURE 1. The faults of gear of the shearer ranging arm.

Because of the mechanical transmission system fault, abnormal changes such as lubricating oil quality, temperature, and mechanical vibration can happen. Therefore, its fault diagnosis is mainly carried out using ferrography analysis, temperature detection, and vibration detection [1], [2]. The ferrography analysis method relies on the experience of human beings, which may cause serious misjudgment because of the irregular spectrum process. The temperature detection method is difficult to achieve early fault diagnosis and accurate fault location of the mechanical transmission system. The vibration detection method can be used to monitor the operating state of equipment without stopping the machine, and to achieve early diagnosis and accurate fault location, which is widely used in the field of fault diagnosis and prediction of mechanical transmission system [3]. In recent decades, the research on fault diagnosis of the mechanical transmission system at home and abroad mainly focuses on evaluating the fault based on vibration intensity and vibration standard, and denoising of vibration signals, and multi-class fault intelligent recognition based on artificial neural network, fuzzy theory or support vector machine [4]–[7]. While, for a complex mechanical transmission system with multiple coincident fault characteristic frequencies, few researchers study on fault location of specific components, especially in the aspect of shearer ranging arm. In engineering practice, accurate fault location of the mechanical transmission system for shearer is very important to reduce unscheduled downtime and greatly improve maintenance efficiency.

The fault diagnosis methods of the mechanical transmission system were explored by some researchers. The fault diagnosis of rotating machinery was carried out using the waveform in the time domain, kurtosis index, and cepstrum [8]. A novel adaptive singular value decomposition (SVD) method is proposed for fault feature detection based on the correlation coefficient [9]. A fast algorithm was proposed for computing the kurtogram, which improves computational efficiency and makes kurtosis applicable to on-line industrial applications [10]. However, the above methods mainly are used to identify the faults, which are difficult to achieve fault location. It is found that there are harmonics of vibration characteristic frequencies and lots of side-bands around the vibration characteristic frequencies. According to the side-bands around the vibration characteristic frequencies, rolling element bearing and gear faults can be identified and located [11]–[13]. Several demodulation methods have been used to extract the side-bands characteristics of vibration signals, such as the Hilbert envelope spectrum analysis method and continuous complex Morlet wavelet envelope demodulation analysis method. The Hilbert envelope spectrum analysis method is used to extract the fault characteristic frequencies of the planetary gearbox, in order to realize the fault identification [14]. The bearing fault is identified by improved Hilbert time-time transform demodulation analysis method [15]. The short-time Fourier transform (STFT) also has its shortcomings. such as STFT only using a single resolution to analyze the target signal [16]. Compared with the method of Hilbert transform demodulation analysis method and short-time Fourier transform method, the continuous complex Morlet wavelet envelope demodulation analysis method can perform envelope analysis in the whole frequency range and eliminate the impact of artificially setting the center frequency, and adjust the time and frequency resolution by changing the center frequency and bandwidth. Compared with the other wavelet transform methods, there is 90° phase difference between the real part and imaginary part in the continuous complex Morlet wavelet envelope demodulation. Moreover, the left and right sides of the Morlet wavelet exhibit exponential attenuation, which is the similar to the characteristic of the shock attenuation waveform of the mechanical fault vibration signal. So, the Morlet wavelet can be used to better match the fault signal [17]. Therefore, according to the principle of envelope demodulation and Morlet wavelet characteristic, the continuous complex Morlet wavelet envelope demodulation method can achieve envelope detection and extract the side-bands characteristics of vibration signals [18]. However, the parameters of continuous complex Morlet wavelet such as center frequency, bandwidth, and scale factor have a large impact on side-bands characteristics extraction [19]. The optimal parameters of continuous complex Morlet wavelet are very difficult to be obtained. Therefore, it needs to deeply study how to obtain the optimal center frequency, bandwidth, and scale factor of Morelet wavelet.

In this study, our main contribution is to propose a combination method of optimized continuous complex Morlet wavelet envelope demodulation spectrum analysis and spectrum analysis to apply to the accurate gear fault location of the mechanical transmission system of shearer ranging arm. In the algorithm, the fault characteristics frequency is obtained by spectrum contrast analysis of vibration signals, and the fault rotation frequency is obtained by the contrast analysis of optimized continuous complex Morlet wavelet envelope demodulation spectrum in normal and fault state. According to the meshing frequency and rotation frequency of gear fault, the fault accurate location of the mechanical transmission system of shearer ranging arm can be obtained. In the algorithm, the optimal center frequency and bandwidth of Morlet wavelet can be obtained by wavelet Shannon entropy, which can get the best time-frequency resolution of vibration signals, and the optimal scale factor is obtained by proposed

spectrum contrast analysis of vibration signals in normal and fault state. Therefore, the optimal Morlet wavelet basis can be selected by the original vibration signals. The proposed method can achieve fault accurate location of the mechanical transmission system of shearer ranging arm. It is of great significance to the safe and efficient production of the coal mine.

II. SIDE-BANDS AROUND THE MESHING FREQUENCY OF GEARS

The vibration signals usually contain multiple harmonics and change with the rotation speed, load, and fault. The changes are presented by the amplitude or phase of vibration signals, which is the modulation phenomenon of vibration signals. When there is a fault in gears, the side-bands usually appear around the meshing frequency of gears and their harmonics. The side-bands imply the fault information, and it is helpful to the fault location. The side-bands are produced because of the modulation. In the modulation, the meshing frequency and its harmonics are carrier frequencies, and the rotation frequency and its multiple frequencies are the modulation frequencies. The vibration signals with modulation are presented in equations (1)∼(3).

$$x(t) = \sum_{m=0}^{M} A_m \left[1 + a_m(t)\right] \cos\left[2\pi m f_z t + \varphi_m + b_m(t)\right] \quad (1)$$

$$a_m(t) = \sum_{n=1}^{N} A_{mn} \cos(2\pi k f_z t + \alpha_m) \quad (2)$$

$$b_m(t) = \sum_{n=1}^{N} B_{mn} \sin(2\pi k f_z t + \beta_m) \quad (3)$$

where, f_z is the meshing frequency of gears, and φ_m is the phase, and A_m is the amplitude, and M is the number of maximum harmonics, and $a_m(t)$ is the function of amplitude modulation, and $b_m(t)$ is the function of phase modulation, and α_m and β_m are the respective initial phase of the nth modulation component.

III. ACCURATE FAULT LOCATION SCHEME AND METHOD OF THE SHEARER RANGING ARM

A. ACCURATE FAULT LOCATION SCHEME OF THE SHEARER RANGING ARM

The combination method of optimized continuous complex Morlet wavelet envelope demodulation spectrum analysis and spectrum analysis is applied to the accurate fault location of the mechanical transmission system of shearer ranging arm. The accurate fault location scheme of shearer ranging arm is presented in Figure 2.

The main processes of accurate fault location are as follows:

(1) The vibration signals in normal and fault states are collected.

(2) The noise reduction of vibration signals is performed by the wavelet transform algorithm.

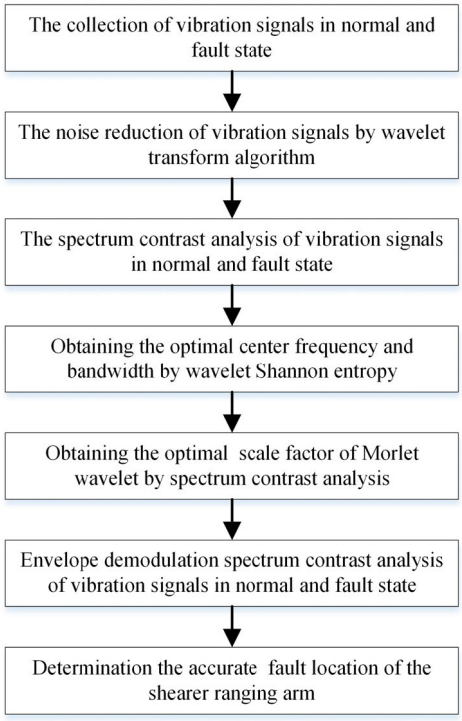

FIGURE 2. The accurate gear fault location scheme of shearer ranging arm.

(3) The spectrum contrast analysis of vibration signals between the normal state and fault state is performed, which can obtain the fault characteristics frequency and preliminary fault location. Due to the same meshing frequency of multiple pairs of gears, it is difficult to precisely locate the faulty gear.

(4) The optimal center frequency and bandwidth are obtained by wavelet Shannon entropy.

(5) The optimal scale factor is obtained by spectrum contrast analysis of vibration signals in normal and fault state.

(6) The envelope demodulation spectrum is obtained by an optimized continuous complex Morlet wavelet envelope demodulation algorithm. The rotation frequency of fault location is got by the contrast analysis of the envelope demodulation spectrum in normal and fault state.

(7) Because different gears have different rotation frequencies, the comprehensive analysis results of optimized continuous complex Morlet wavelet envelope demodulation spectrum and spectrum can uniquely determine the fault location of gears.

B. ACCURATE FAULT LOCATION METHOD OF THE SHEARER RANGING ARM

1) THE ENVELOPE DEMODULATION THEORY OF CONTINUOUS COMPLEX MORLET WAVELET

The envelope demodulation theory of continuous complex Morlet wavelet is presented as follows [20]–[22]:

The wavelet basis is obtained from the ''mother wavelet'' $\psi(t)$ by translation and dilation, which is presented in

Equation (4).

$$\psi_{a,b}(t) = \frac{1}{\sqrt{a}}\psi\left(\frac{t-b}{a}\right) \tag{4}$$

where, a is the scale factor, and b is the time localization parameter.

According to the principle of the wavelet transform, the wavelet transform of a finite energy signals $x(t)$ can be operated by a convolution between $x(t)$ and the wavelet basis $\psi_{a,b}(t)$,which is presented in Equation (5).

$$W(a,b) = |a|^{-1/2}\int_{-\infty}^{+\infty} x(t)\psi^*_{a,b}(\frac{t-b}{a})dt \tag{5}$$

where $\psi^*(t)$ is the complex conjugate of $\psi_{a,b}(t)$.

The continuous complex Morlet wavelet function in time domain is presented in Equation (6).

$$\psi(t) = \frac{1}{\sqrt{\pi f_b}}e^{-t^2/f_b}e^{j2\pi f_c t} \tag{6}$$

where, f_c and f_b determine the center frequency and bandwidth of the wavelet window.

According to the Equation (6), the continuous complex Morlet wavelet function in frequency domain is presented in Equation (7).

$$\varphi(f) = \frac{1}{\sqrt{\pi f_b}}e^{-\pi^2 f_b(f-f_c)} \tag{7}$$

According to the Equation (6), the real part $\psi_r(t)$ and the imaginary part $\psi_i(t)$ of the continuous complex Morlet wavelet are presented in Equations (8) and (9), respectively.

$$\psi_r(t) = \frac{1}{\sqrt{\pi f_b}}e^{-t^2/f_b}\cos(2\pi f_c t) \tag{8}$$

$$\psi_i(t) = \frac{1}{\sqrt{\pi f_b}}e^{-t^2/f_b}\sin(2\pi f_c t) \tag{9}$$

According to the principle of wavelet transform, Morlet wavelet envelope demodulation signals $W(a,b)$ with different scale factors can be obtained by convolution of reality signals $x(t)$ and continuous complex Morlet wavelet with Shrinking transformation, which is presented in Equation (10).

$$\begin{aligned} W(a,b) &= x(t) * \frac{1}{a}\psi(t/a) \\ &= x(t) * \frac{1}{a}\psi_r(t/a) + x(t) * j\frac{1}{a}\psi_i(t/a) \end{aligned} \tag{10}$$

Based on the real part and imaginary part of the continuous complex Morlet wavelet in Equations (8) and (9), the real part and imaginary part of $W(a,b)$ are presented in Equations (11) and (12), respectively.

$$\mathrm{Re}[W(a,b)] = \frac{1}{\sqrt{\pi f_b}}e^{-(t/a)^2/f_b}\cos(2\pi f_c t/a) \tag{11}$$

$$\mathrm{Im}[Wf(a,b)] = x(t) * \frac{1}{\sqrt{\pi f_b}}e^{-(t/a)^2/f_b}\sin(2\pi f_c t/a) \tag{12}$$

According to Equations (11) and (12), the Morlet wavelet envelope signals $u(a,t)$ with different scale factors is presented in Equations (13).

$$u(a,t) = \sqrt{\mathrm{Re}^2[W(a,b)] + \mathrm{Im}^2[W(a,b)]} \tag{13}$$

By performing Fourier transform on the Morlet wavelet envelope signals $u(a,t)$ with different scale factors, the continuous complex Morlet wavelet envelope demodulation spectrum with different scale factors can be obtained.

2) OBTAINING THE OPTIMAL CENTER FREQUENCY AND BANDWIDTH BY WAVELET SHANNON ENTROPY

We hope the Morlet wavelet basis function has the greatest similarity with vibration signals. The wavelet Shannon entropy is a good evaluation criterion for signals similarity, which reflects the uniformity of the probability distribution. Therefore, the optimal center frequency f_c and bandwidth parameter f_b of Morlet wavelet are obtained by Wavelet Shannon entropy. The most uncertain probability distribution has the largest entropy value. The smaller the entropy value, the better the corresponding Morlet wavelet basis function matches the vibration signals. The wavelet Shannon entropy is presented in Equation(14) [23].

$$\begin{aligned} H^{u,v}(P) &= -\sum_{i=1}^{N} P_i^{u,v}\ln P_i^{u,v} \\ f_c &= u \in [J,U], \quad f_b = v \in [K,V] \end{aligned} \tag{14}$$

where, $\sum_{i=1}^{N} P_i^{u,v} = 1$, P_i is the uncertain probability distribution, which is presented in Equation(15).

$$P_i^{u,v} = |W(a_i,t)| \Big/ \sum_{j=1}^{M} \left|W\left(a_j,t\right)\right| \tag{15}$$

where, $W(a_i,t)$ is the wavelet transform coefficients of a_i scale.

3) OBTAINING THE OPTIMAL SCALE FACTOR OF MORLET WAVELET BY SPECTRUM CONTRAST ANALYSIS

The relationship between scale and characteristic frequency of vibration signals is presented in Equation (16). According to the comparative analysis of the spectrum in normal and fault state, the characteristic frequency of the fault can be determined. In order to accurately perform the morlet wavelet transform, the corresponding transform scale is found by the determined characteristic frequency. The scale corresponding to the fault characteristic frequency of vibration signals is the optimal scale.

$$f_i = f_c \times f_s/a_i \tag{16}$$

where, f_i is the gear meshing frequency, f_s is the sampling frequency, a_i is the scale, and f_c is the center frequency.

IV. THE INFLUENCE ANALYSIS OF CENTER FREQUENCY AND BANDWIDTH BY SIMULATE SIGNALS

A. THE TIME AND FREQUENCY RESOLUTION OF MORLET WAVELET

Time and frequency resolution of mother wavelet is presented in Equation (17) and Equation (18). Δt_{ai} is the time resolution of mother wavelet when the scale is a_i. Δf_{ai} is the frequency resolution of mother wavelet when the scale is a_i. The larger Δt_{ai} is, the worse time resolution is. The larger Δf_{ai} is, the worse frequency resolution is.

$$\Delta t_i = \frac{\sqrt{f_b}}{2}, \quad \Delta f_i = \frac{1}{2\pi\sqrt{f_b}} \tag{17}$$

$$\Delta t_{ai} = a_i \Delta t_i = \frac{f_c \cdot f_s}{f_i} \frac{\sqrt{f_b}}{2}$$

$$\Delta f_{ai} = \frac{1}{a_i} \Delta f_i = \frac{f_i}{f_c \cdot f_s} \frac{1}{2\pi\sqrt{f_b}} \tag{18}$$

where, f_i is the gear meshing frequency, f_s is the sampling frequency, a_i is the scale, f_b is the bandwidth parameter, and f_c is the center frequency.

B. THE TIME-FREQUENCY RESOLUTION CONTRAST ANALYSIS WITH DIFFERENT f_c AND f_b

In order to verify the effect of parameters f_c and f_b on time and frequency resolution, the simulation signals of fault shock is presented in Equation(19).

$$\begin{aligned} x(t) = & \exp(-(t-400)^2/200)\cos(2\pi(t-400)/10) \\ & + \exp(-(t-425)^2/200)\cos(2\pi(t-425)/15) \\ & + \exp(-(t-440)^2/200)\cos(2\pi(t-440)/10) \end{aligned} \tag{19}$$

The simulation signals are composed by three components with the frequency of 1/10Hz, 1/10Hz, and 1/15Hz, and the phases of three components are different. The time domain waveform of simulation signal is presented in Figure 3. Based on the simulation signals of fault shock, the optimal center frequency f_c and bandwidth parameter f_b are obtained by wavelet Shannon entropy, which is presented as follows:

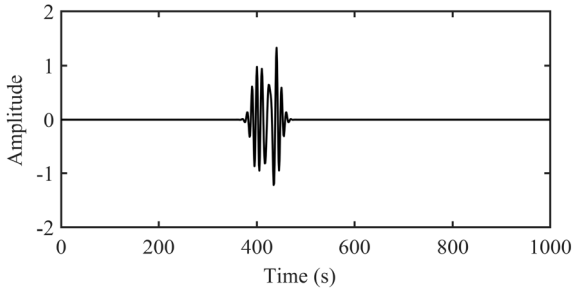

FIGURE 3. The time domain waveform of simulation signal.

The range of f_c is set as [0.05, 0.7], and the step size is 0.05. The range of f_b is set as [0.5, 50], and the step size is 0.5. The relationship between wavelet Shannon entropy and center frequency f_c, bandwidth parameter f_b can be obtained, which is presented in Figure 4 by three-dimensional plot. As can be observed in Figure 4, the minimum entropy value

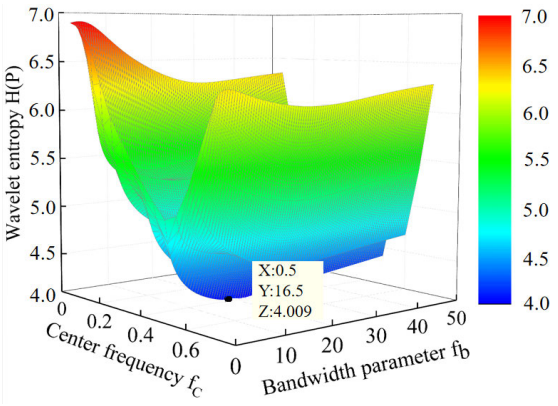

FIGURE 4. The three-dimensional relationship between wavelet Shannon entropy and center frequency f_c, bandwidth parameter f_b.

TABLE 1. The time and frequency resolution with different f_b.

Resolution / fc , fb	Time resolution	Frequency resolution
fc=0.5, fb=5	8.385	0.0095
fc=0.5, fb=16.5	15.233	0.0052
fc=0.5, fb=95	36.545	0.0022

forms a "ridge-line" at the bottom along with the changes of f_c and f_b, and the value of Shannon entropy is minmum with $f_c = 0.5$ and $f_b = 16.5$. Therefore, the optimal center frequency and bandwidth of the Morlet wavelet are $f_c = 0.5$ and $f_b = 16.5$.

The time-frequency image contrast of simulation signals using continuous Morlet wavelet with $f_c = 0.5$ and $f_b = 5/16.5/95$ is presented in Figure 5. And, the time resolution and frequency resolution can be obtained by Equation (18), which are presented in Table 1. According to equation (19), the simulation signal is composed of three components with the frequency of 1/10Hz, 1/10Hz, and 1/15Hz, and the phases of three components are different. As can be observed in Figure 5(b), the time and frequency resolution are the most suitable with $f_c = 0.5$ and $f_b = 16.5$, because the three components of simulation signal are completely separated in time and frequency direction. As can be observed in Figure 5(a) and Table 1, the three components of simulation signal are separated in time direction, but two components with frequency 1/10Hz and 1/15Hz are not separated in frequency direction. Because the frequency resolution in Figure 5(a) is lower than in Figure 5(b). As can be observed in Figure 5(c) and Table 1, the three components of simulation signal separated in frequency direction, but two components of frequency 1/10Hz with different phase are not separated in time direction. Because the time resolution in Figure 5(c) is lower than in Figure 5(b).

The time-frequency image contrast of simulation signals using continuous Morlet wavelet with $f_c = 0.2/0.5/0.8$ and $f_b = 16.5$ is presented in Figure 6. And, the time resolution and frequency resolution can be obtained by Equation (18),

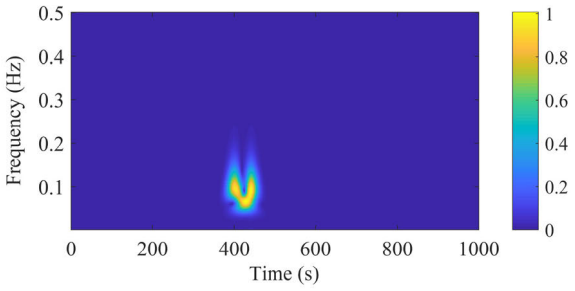

(a) $f_c = 0.5, f_b = 5$

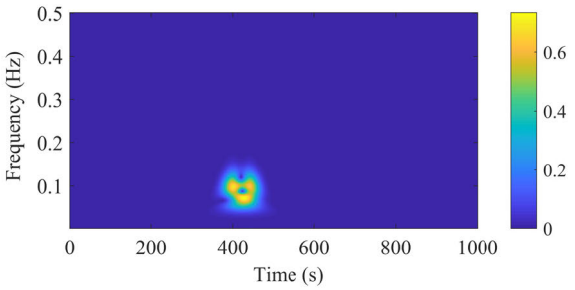

(b) $f_c = 0.5, f_b = 16.5$

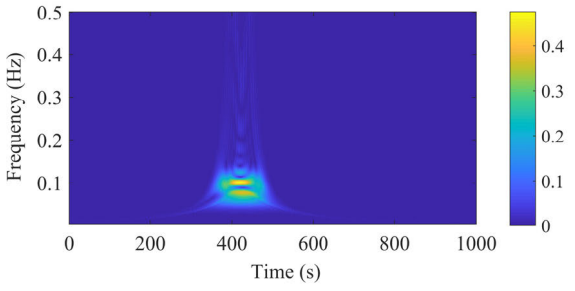

(c) $f_c = 0.5, f_b = 95$

FIGURE 5. The time-frequency image with $f_c = 0.5$ and $f_b = 5/16.5/95$.

TABLE 2. The time and frequency resolution with different f_c.

Resolution / fc , fb	Time resolution	Frequency resolution
fc=0.2, fb=16.5	6.093	0.0131
fc=0.5, fb=16.5	15.233	0.0052
fc=0.8, fb=16.5	24.372	0.0033

which are presented in Table 2. The simulation signal is composed of three components with the frequency of 1/10Hz, 1/10Hz, and 1/15Hz, and the phases of three components are different. As can be observed in Figure 6(b), the time and frequency resolution are the most suitable with $f_c = 0.5$ and $f_b = 16.5$, because the three components of simulation signal are completely separated in time and frequency direction. As can be observed in Figure 6(a) and Table 2, the three components of simulation signal are separated in time direction, but two components with frequency 1/10Hz and 1/15Hz are not separated in frequency direction. Because the frequency

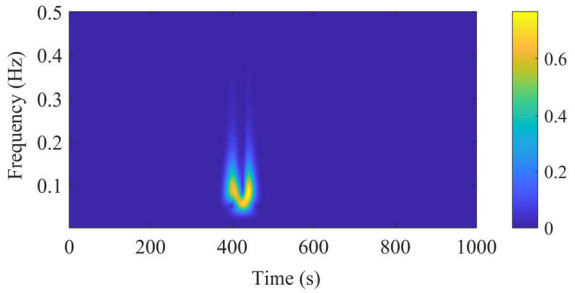

(a) $f_c = 0.2, f_b = 16.5$

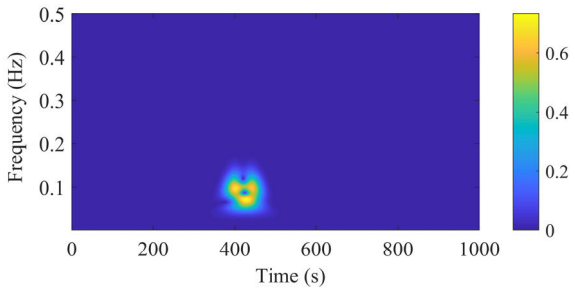

(b) $f_c = 0.5, f_b = 16.5$

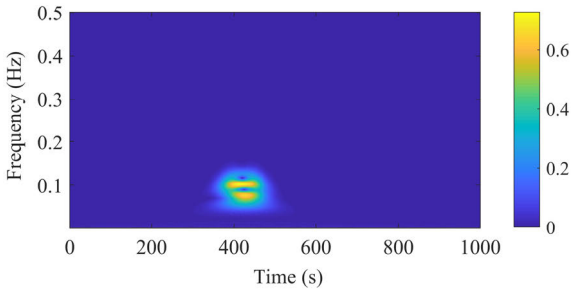

(c) $f_c = 0.8, f_b = 16.5$

FIGURE 6. The time-frequency image with $f_c = 0.2/0.5/0.8$ and $f_b = 16.5$.

resolution in Figure 6(a) is lower than in Figure 6(b). As can be observed in Figure 6(c) and Table 2, the three components of simulation signal separated in frequency direction, but two components of frequency 1/10Hz with different phase are not separated in time direction. Because the time resolution in Figure 6(c) is lower than in Figure 6(b).

In summary, the time resolution and frequency resolution with the center frequency $f_c = 0.5$ and the bandwidth $f_b = 16.5$ obtained by wavelet Shannon entropy is the best. Therefore, the simulation results indicate that the best time and frequency resolution of Morlet can be obtained by wavelet Shannon entropy, which can make the wavelet waveform best match the fault impact signal.

V. EXPERIMENTAL RESULTS AND DISCUSSION

DH186E vibration acceleration sensors with the sensitivity 9.97mv/m $\cdot$ s^{-2} and DH5901 vibration tester were used to collect the vibration signals of MG1480 and MG1660 shearer

ranging arm in normal and fault state. The vibration sensors were fixed on the ranging arm of shearer by a magnetic suction base. In order to verify the proposed accurate gear fault location method, the MG1480 and MG1660 shearer are used to experimental verification.

A. EXPERIMENTAL VERIFICATION OF MG1480 SHEARER FAULT LOCATION

1) COLLECTION OF VIBRATION SIGNALS IN NORMAL AND FAUIT STATE

The vibration sensors layout of the MG1480 shearer ranging arm was presented in Figure 7. As can be observed, the vibration sensors are arranged 4 axial positions and 4 radial positions, respectively. By comprehensive analysis of vibration detection signals at different positions, the axial vibration signals of the idler shaft obviously change in normal and fault state. So, the axial vibration signals of the idler shaft is used to fault location analysis.

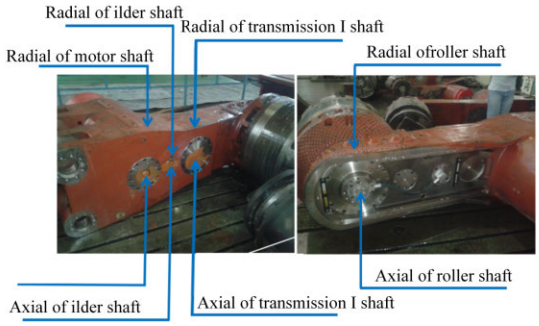

FIGURE 7. Vibration sensor layout of MG1480 shearer.

2) THE CONTRAST ANALYSIS OF THE TIME DOMAIN SIGNALS BEFORE AND AFTER NOISE REDUCTION

In fault diagnosis of mechanical transmission system, Daubechies wavelet is usually applied [24]. By noise reduction experiment, the db17 wavelet basis and the decomposition layer for 5 are determined to noise reduction of the axial vibration signals of idler shaft. The time domain signals of MG1480 shearer normal ranging arm and fault ranging arm before and after noise reduction are presented in Figure 8. As can be observed in Figure 8, the wavelet transform method has good noise reduction effeteness. The maximum absolute value of vibration amplitude for normal ranging arm after noise reduction is 376.5m/s^2. While, the maximum absolute value of vibration amplitude for fault ranging arm after noise reduction is 687.8m/s^2, which is much larger than the vibration amplitude of normal ranging arm.

3) THE CONTRAST ANALYSIS OF SPECTRUM IN NORMAL AND FAULT STATE AFTER NOISE REDUCTION

The mechanical transmission system of MG1480 shearer ranging arm is presented in Figure 9. The synchronous rotation speed of the motor is 1500r/min. The gears vibration characteristic frequencies of MG1480 shearer ranging arm

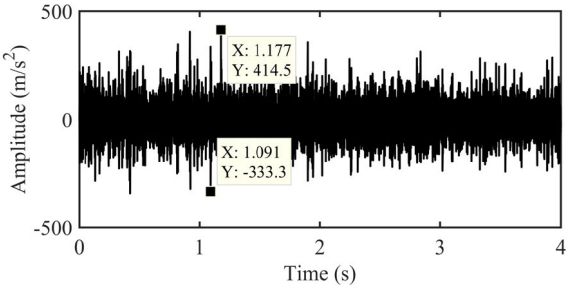

(a) The vibration signals of normal ranging arm before noise reduction

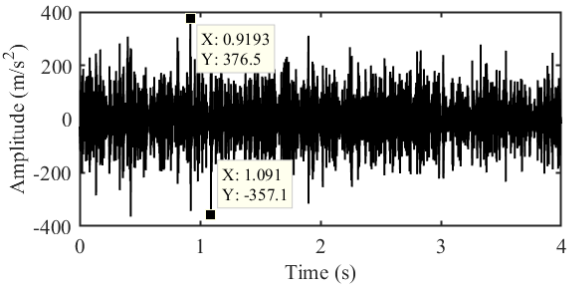

(b) The vibration signals of normal ranging arm after noise reduction

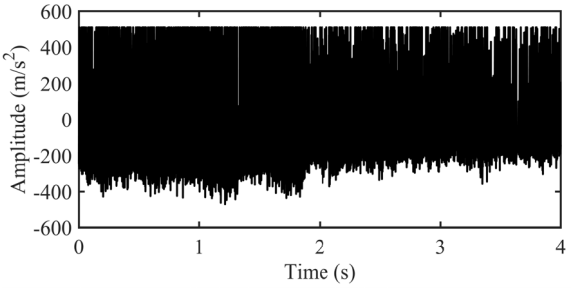

(c) The vibration signals of fault ranging arm before noise reduction

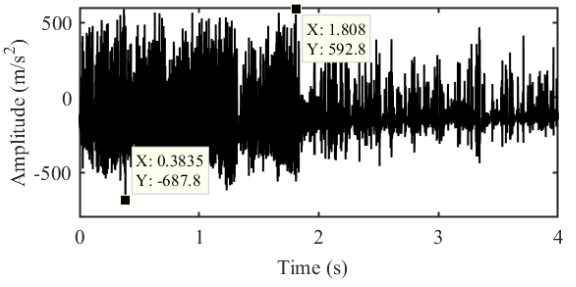

(d) The vibration signals of fault ranging arm after noise reduction

FIGURE 8. The contrast of vibration signals between normal ranging arm and fault ranging arm.

can be obtained and presented in Table 3. The key vibration characteristic frequencies of gears are meshing frequency and rotation frequency.

The contrast of spectrum between normal ranging arm and fault ranging arm for MG1480 shearer is presented in Figure 10. The contrast of amplitudes at the key frequencies between normal ranging arm and fault ranging arm

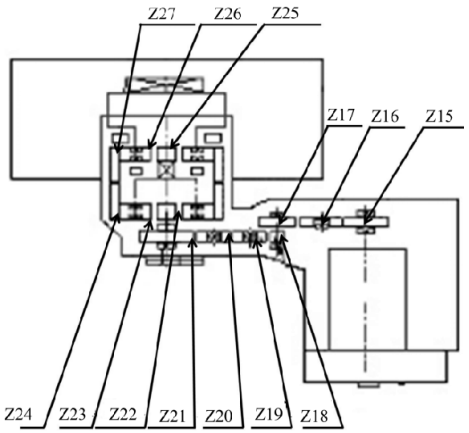

FIGURE 9. Mechanical transmission system of MG1480 shearer ranging arm.

TABLE 3. The gears vibration characteristic frequencies of MG1480 shearer ranging arm.

Gear number	Z15	Z16	Z17	Z18	Z19	Z20
Rotation frequency (Hz)	25	17.95	17.5	17.5	14.32	14.32
Meshing frequency (Hz)	700	700	700	472.5	472.5	472.5
Gear number	Z21	Z22	Z23	Z24	Z25	Z26
Rotation frequency (Hz)	11.81	11.81	7.88	0	2.36	1.85
Meshing frequency (Hz)	472.5	189	189	0	42.5	42.5

TABLE 4. The amplitudes contrast of spectrum at key frequencies of MG1480 shearer ranging arm.

Frequency(Hz)	472.5	700	945	1400	1890
Amplitude(m/s^2) in normal state	0.218	3.671	2.324	17.83	0.7769
Amplitude(m/s^2) in fault state	9.661	1.857	4.413	16.95	5.05
Fault state/normal state	44.32	0.51	1.90	0.95	6.50

can be obtained by Figure 10 and are presented in Table 4. As can be observed, the amplitudes at the 472.5Hz and its frequency multiplications are much larger in fault state than in the normal state. Especially at 472.5Hz, the amplitude in fault state is 44.32 times the normal state. While the amplitudes at the 700Hz and its 2 times frequency are smaller in fault state than in the normal state. So, the fault is located at the meshing frequency of 472.5Hz. Therefore, the fault may occur at one or more gears in Z18, Z19, Z20, and Z21, and the rotation frequency of fault gear may be 17.5Hz, 14.32Hz, or 11.81Hz. It can be seen that the spectrum analysis does not accurately locate the specific location of the fault.

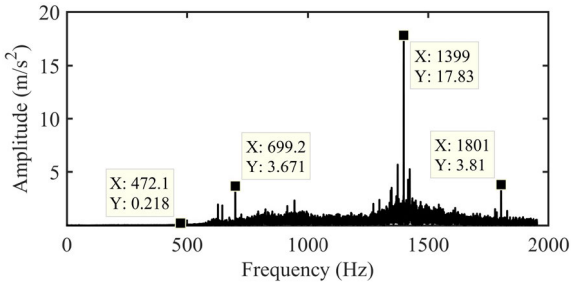

(a) The vibration signals spectrum of normal ranging arm

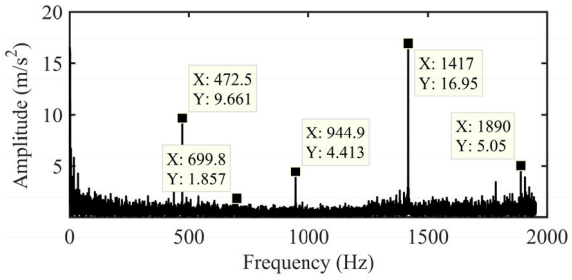

(b) The vibration signals spectrum of fault ranging arm

FIGURE 10. The contrast of spectrum between normal ranging arm and fault ranging arm for MG1480 shearer.

4) THE CONTRAST ANALYSIS OF MORLET WAVELET ENVELOPE DEMODULATION SPECTRUM

Based on the vibration signals of MG1480 shearer, the optimal center frequency f_c and bandwidth parameter f_b are obtained by wavelet Shannon entropy, which are presented as follows:

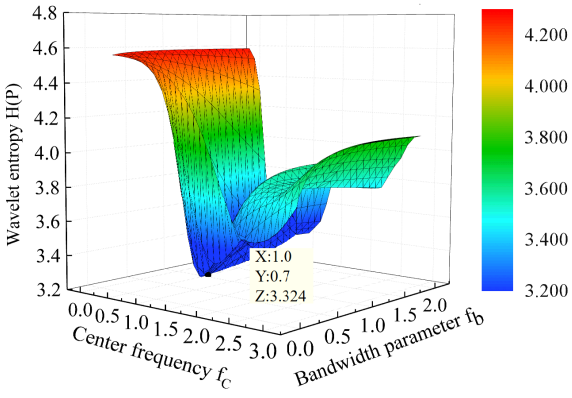

FIGURE 11. The three-dimensional relationship between wavelet Shannon entropy and center frequency f_c, bandwidth parameter f_b.

The range of f_c is set as [0.1, 3.0] and the step size is 0.1. The range of f_b is set as [0.1, 2.0], and the step size is 0.1. The relationship between wavelet Shannon entropy and center frequency f_c, bandwidth parameter f_b can be obtained, which is presented in Figure 11 by three-dimensional plot. As can be observed in Figure 11, the minimum entropy value forms a ''ridge-line'' at the bottom along with the changes of f_c and f_b, and the value of Shannon entropy is minimum with

TABLE 5. The amplitude contrast of Morlet wavelet envelope demodulation spectrum of MG1480 shearer.

Frequency(Hz)	17.5	35(2 times of 17.5)
Amplitude(m/s^2) in normal state	0.4357	0.4816
Amplitude(m/s^2) in fault state	7.046	5.438
Fault state/normal state	16.17	11.29

$f_c = 1.0, f_b = 0.7$. Therefore, the optimal center frequency and bandwidth of the Morlet wavelet are $f_c = 1.0, f_b = 0.7$.

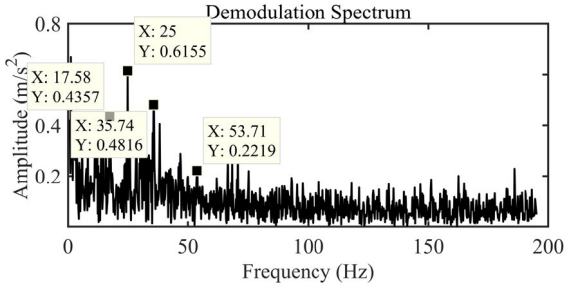

(a) Morlet wavelet envelope demodulation spectrum of normal ranging arm

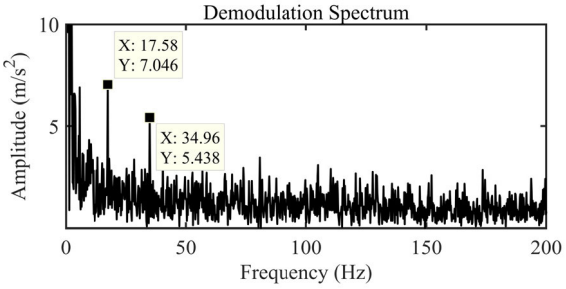

(b) Morlet wavelet envelope demodulation spectrum of fault ranging arm

FIGURE 12. The contrast of Morlet wavelet envelope demodulation spectrum of MG1480 shearer.

The sampling frequency is 51200Hz, and the center frequency $f_c = 1$, and the fault frequency is 472.5Hz. Therefore, according to Equation (18), the optimal scale of the Morlet wavelet envelope demodulation is 108. According to the optimal center frequency, bandwidth and scale of Morlet wavelet, the envelope demodulation spectrum of normal ranging arm and fault ranging arm is presented in Figure 12 and Table 5. As can be observed, the amplitude of 17.5Hz and 2 times frequency in the fault state is 16.17 and 11.29 times the normal state, respectively. Therefore, the rotation frequency of faulty gear is 17.5Hz, and the is fault located at one or more gears in Z17 and Z18.

5) THE ACCURATE FAULT LOCATION

The gear fault can be accurately located by the meshing frequency and rotation frequency. The meshing frequency of gear fault can be obtained by the spectrum contrast analysis in the normal state and fault state, and the rotation frequency of gear fault can be obtained by the contrast analysis of the envelope demodulation spectrum in normal and fault state.

According to the spectrum contrast analysis in the normal state and fault state in Figure 10, the gear fault is located at the meshing frequency of 472.5Hz. According to the contrast analysis of the envelope demodulation spectrum in normal and fault state in Figure 12, the gear fault is located at the rotation frequency of 17.5Hz. By the comprehensive contrast of the spectrum and Morlet wavelet envelope demodulation spectrum, As can be observed in Table 3, the fault is located at Z18 gear. Because the meshing frequency and rotation frequency of Z18 gear is 472.5Hz and 17.5Hz, respectively. The reality is that there is an abrasion fault at Z18 gear, which is presented in Figure 13. The results of fault diagnosis indicate that the fault of the mechanical transmission system for the MG1480 shearer ranging arm has been accurately located by the combination method of optimized continuous complex Morlet wavelet envelope demodulation spectrum analysis and spectrum contrast analysis between the normal state and the fault state.

FIGURE 13. The abrasion fault at Z18 gear.

B. EXPERIMENTAL VERIFICATION OF MG1660 SHEARER FAULT LOCATION

1) COLLECTION OF VIBRATION SIGNALS IN NORMAL AND FAUIT STATE

The vibration sensors layout of MG1660 shearer ranging arm was presented in Figure 14. As can be observed, the vibration sensors are arranged 8 positions which are axial and radial of the motor shaft, idler shaft, transmission I shaft, and roller shaft. By comprehensive analysis of vibration detection signals at different positions, the axial vibration signals of the idler shaft obviously change in normal and fault state. So, the axial vibration signals of the idler shaft is used to fault location analysis.

2) THE CONTRAST ANALYSIS OF VIBRATION SIGNALS OF MG1660 SHEARER BEFORE AND AFTER NOISE REDUCTION

The mechanical transmission system of the MG1660 shearer ranging arm is presented in Figure 15. The synchronous

rotation speed of the motor is 1500r/min. The gears vibration characteristic frequencies of MG1660 shearer ranging arm can be obtained and presented in Table 6. The key vibration characteristic frequencies of gears are meshing frequency and rotation frequency.

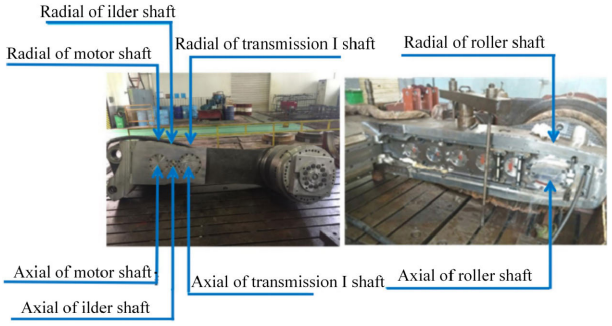

FIGURE 14. Vibration sensor layout of the MG1660 shearer ranging arm.

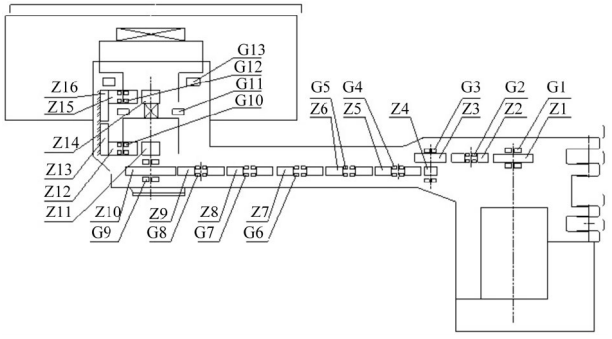

FIGURE 15. Mechanical transmission system of MG1660 shearer ranging arm.

The contrast analysis of axial vibration signals for the idler shaft in the time domain between normal ranging arm and fault ranging arm is presented as follows:

The wavelet transform with db17 wavelet basis and the decomposition layer for 5 is used to noise reduction of the axial vibration signals of the idler shaft. The time-domain signals of MG1660 shearer normal ranging arm and fault ranging arm before and after noise reduction are presented in Figure 16. As can be observed in Figure 16, the wavelet transform method has good noise reduction effeteness. The maximum absolute value of vibration amplitude for normal ranging arm after noise reduction is 359.9m/s^2. While, the maximum absolute value of vibration amplitude for fault ranging arm after noise reduction is 933.3m/s^2, which is much larger than the vibration amplitude of normal ranging arm.

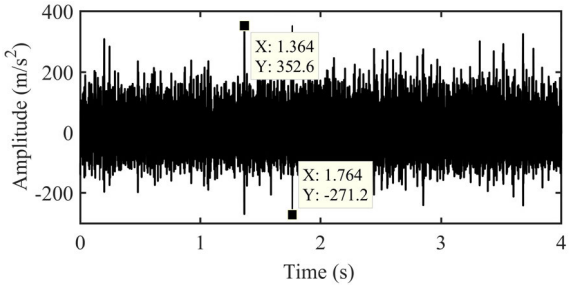

(a) The vibration signals of normal ranging arm before noise reduction

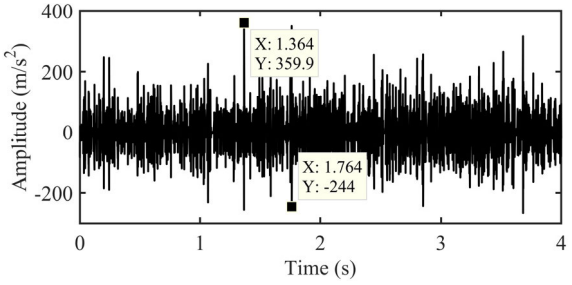

(b) The vibration signals of normal ranging arm after noise reduction

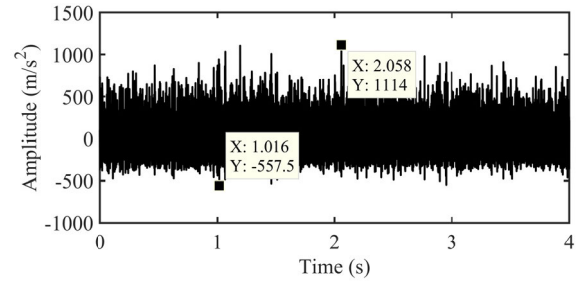

(c) The vibration signals of fault ranging arm before noise reduction

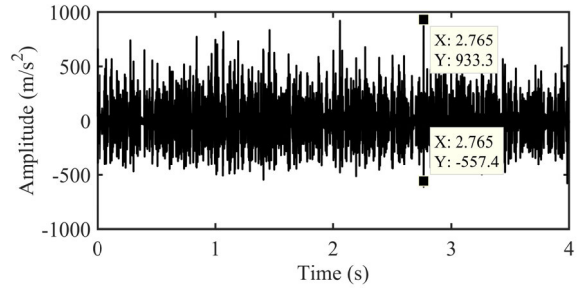

(d) The vibration signals of fault ranging arm after noise reduction

FIGURE 16. The contrast of vibration signals between normal ranging arm and fault ranging arm.

3) THE CONTRAST ANALYSIS OF SPECTRUM IN NORMAL AND FAULT STATE AFTER NOISE REDUCTION

The contrast of amplitudes at the key frequencies between normal ranging arm and fault ranging arm can be obtained by Figure 17 and are presented in Table 7. As can be observed, the vibration of amplitudes at the approximate 525Hz and its frequency multiplications are much larger in fault state than in the normal state. Especially at the approximate 525Hz, the amplitude in fault state is 11.09 times the normal state. The fault is located at the meshing frequency of 525Hz. Therefore, the fault is located at one or more gears in Z1, Z2, and Z3, and the rotation frequency of fault gear may be 25Hz, 20.2Hz, or 18.1Hz. It can be seen that the spectrum analysis does not accurately locate the specific location of the fault.

TABLE 6. The gears vibration characteristic frequencies of MG1660 shearer ranging arm.

Gear number	Z1	Z2	Z3	Z4	Z5	Z6	Z7	Z8
Rotation frequency(Hz)	25	20.2	18.1	18.1	12.5	12.9	12.5	12.5
Meshing frequency(Hz)	525	525	525	362	362	362	362	362
Gear number	Z9	Z10	Z11	Z12	Z13	Z14	Z15	Z16
Rotation frequency(Hz)	12.9	12.07	12.1	10.1	0	2.8	2.4	0
Meshing frequency(Hz)	362.1	362.1	313.8	313.8	0	66.1	66.1	0

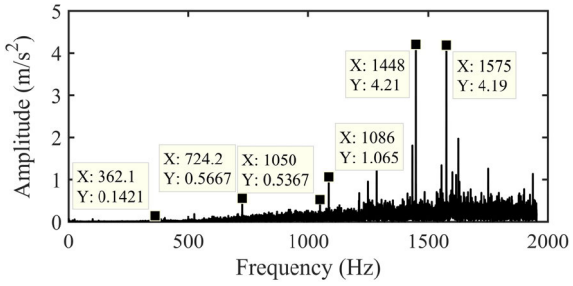

(a) The vibration signals spectrum of normal ranging arm

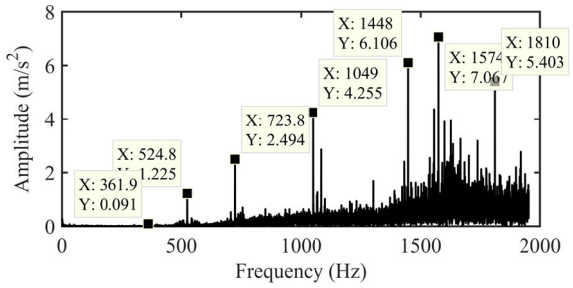

(b) The vibration signals spectrum of fault ranging arm

FIGURE 17. The contrast of spectrum between normal ranging arm and fault ranging arm for MG1660 shearer.

TABLE 7. Contrast of spectrum amplitudes at key frequencies of MG1660 shearer ranging arm.

Frequency (Hz)	362	525	724	1050	1448	1575
Amplitude (m/s^2) in normal state	0.14	0.11	0.5667	0.5353	4.21	4.19
Amplitude (m/s^2) in fault state	0.09	1.23	2.494	4.255	6.106	7.067
Fault state/normal state	0.64	11.09	4.4	7.95	1.45	1.68

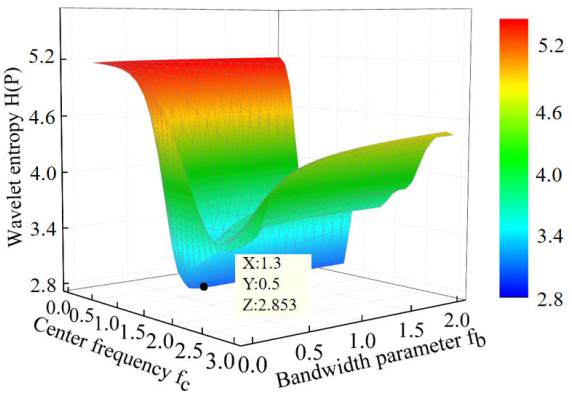

FIGURE 18. The three-dimensional relationship between wavelet Shannon entropy and center frequency f_c, bandwidth parameter f_b.

4) THE CONTRAST ANALYSIS OF MORLET WAVELET ENVELOPE DEMODULATION SPECTRUM

The range of f_c is set as [0.1, 3.0] and the step size is 0.1. The range of f_b is set as [0.1, 2.0], and the step size is 0.1. The relationship between wavelet Shannon entropy and center frequency f_c, bandwidth parameter f_b can be obtained, which is presented in Figure 18 by three-dimensional plot. As can be observed in Figure 18, the minimum entropy value forms a ''ridge-line'' at the bottom along with the changes of f_c and f_b, and the value of Shannon entropy is minimum with $f_c = 1.3, f_b = 0.5$. Therefore, the optimal center frequency and bandwidth of the Morlet wavelet are $f_c = 1.3, f_b = 0.5$.

For the MG1660 shearer, the sampling frequency is 51200Hz, and the center frequency $f_c = 1.3$, and the fault frequency is 525Hz. Therefore, according to Equation (18), the optimal scale of Morlet wavelet envelope demodulation is 127. According to the optimal center frequency, bandwidth and scale of Morlet wavelet, the envelope demodulation spectrum of normal ranging arm and fault ranging arm for MG1660 shearer is presented in Figure 19 and Table 8. As can be observed, the key frequencies are approximate 18.10Hz, 20.19Hz, 25Hz, and frequency multiplications of 18.1Hz and 20.19Hz. Especially at the approximate 18.10Hz, the amplitude in fault state is 10.64 times the normal state. While the amplitudes at the approximate 20.19Hz and 25Hz and their 2 times frequency are close in fault state and in normal state. So, the fault is located at the rotation frequency

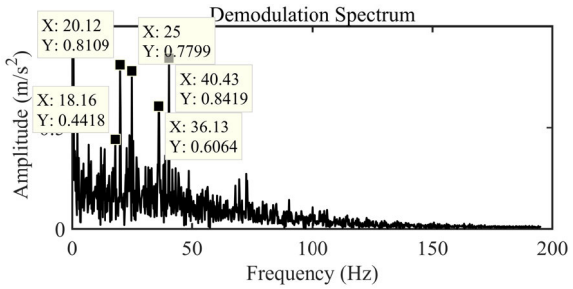

(a) Morlet wavelet envelope demodulation spectrum of normal ranging arm

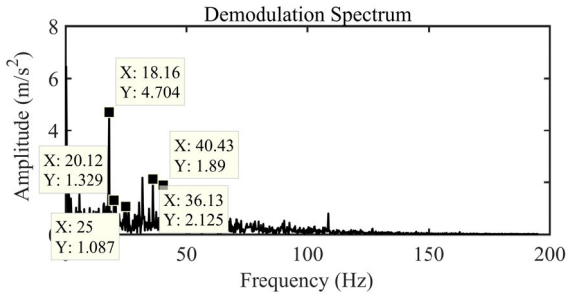

(b) Morlet wavelet envelope demodulation spectrum of fault ranging arm

FIGURE 19. The contrast of Morlet wavelet envelope demodulation spectrum between normal ranging arm and fault ranging arm of MG1660 shearer.

TABLE 8. The amplitude contrast of Morlet wavelet envelope demodulation spectrum of MG1660 shearer.

Frequency(Hz)	18.1	20.2	25	36.2	40.4
Amplitude (m/s^2) in normal state	0.4418	0.8109	0.7799	0.6087	0.8419
Amplitude (m/s^2) in fault state	4.704	1.329	1.087	2.125	1.89
Fault state/normal state	10.64	1.63	1.39	3.49	2.24

of 18.10Hz. Therefore, the fault is located at one or more gears in Z3 and Z4.

5) THE ACCURATE FAULT LOCATION

The gear fault can be accurately located by the meshing frequency and rotation frequency. The meshing frequency of gear fault can be obtained by the spectrum contrast analysis in the normal state and fault state, and the rotation frequency of gear fault can be obtained by the contrast analysis of the envelope demodulation spectrum in normal and fault state.

According to the spectrum contrast analysis in the normal state and fault state in Figure 17, the gear fault is located at the meshing frequency of 525Hz. According to the contrast analysis of the envelope demodulation spectrum in normal and fault state in Figure 19, the gear fault is located at the rotation frequency of 18.10Hz. By the comprehensive contrast of the spectrum and Morlet wavelet envelope demodulation spectrum, As can be observed in Table 6, the fault is located

FIGURE 20. The partial meshing at Z3 gear because of tooth shape and tooth direction error.

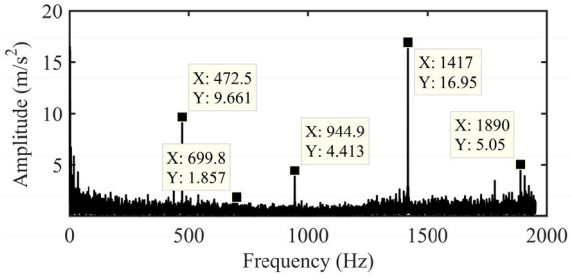

(a) The spectrum for the axial vibration signals of idler shaft for MG1480 shearer in fault state

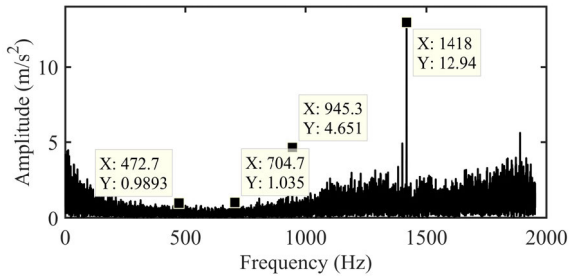

(b) The spectrum for the axial vibration signals of roller shaft for MG1480 shearer in fault state

FIGURE 21. The contrast of spectrum between the axial vibration signals of roller shaft and idler shaft for MG1480 shearer.

at Z3 gear. Because the meshing frequency and rotation frequency of Z3 gear is 525Hz and 18.10Hz, respectively.The real fault is that the tooth profile error of the Z3 gear is 23.2 μm and the tooth direction error is 32.2 μm. Because of the tooth profile error and tooth direction of the Z3 gear, the Z3 gear is caused to wear by the partial meshing of the Z2 and Z3 gears.The Z3 gear with partial meshing is presented in Figure 20. The results of fault diagnosis indicate that the fault of the mechanical transmission system for the MG1660 shearer ranging arm has been accurately located by the combination method of optimized continuous complex Morlet wavelet envelope demodulation spectrum analysis and spectrum analysis between the normal state and the fault state.

C. DISCUSSION

The vibration sensors layout of the MG1480 shearer ranging arm was presented in Figure 7. The contrast of amplitudes at the key frequencies between the axial vibration signals of the roller shaft and the axial vibration signals of the idler shaft

are presented in Figure 21. As can be observed in Figure 21, the amplitudes of the axial vibration signals of idler shaft at the key frequency are much larger than the axial vibration signals of the roller shaft, and the meshing frequency 472.5Hz was severely submerged. Because the sensor of the axial vibration signals for the roller shaft is far away from the corresponding to meshing frequency of 472.5Hz, and the vibration signal amplitude reduction after a long transmission path. So, in order to detect the fault of the low-speed shaft and the high-speed shaft of the shearer ranging arm, it is necessary to at least arrange the sensors at the idler and roller shaft.

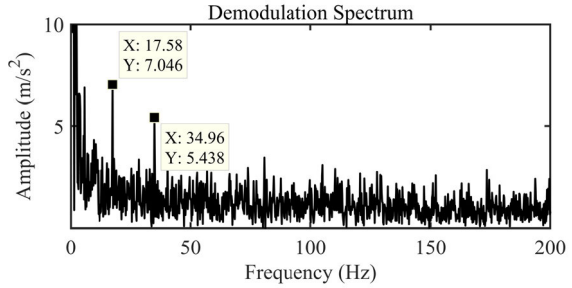

(a) Morlet wavelet envelope demodulation spectrum of fault ranging arm

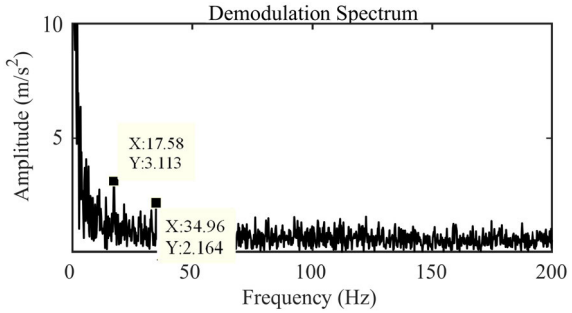

(b) Hilbert envelope spectrum of fault ranging arm

FIGURE 22. Comparison of optimized complex Morlet wavelet envelope demodulation spectrum and Hilbert envelope spectrum of MG1480 shearer.

The optimized complex Morlet wavelet envelope demodulation spectrum and the Hilbert envelope spectrum are presented in Figure 22(a) and 22(b), respectively. As can be observed, the characteristic frequency of 17.5Hz and the double frequency of 17.5Hz in Figure 22(a) are more obvious than those in Figure 22(b). And the double frequency characteristic of 17.5Hz in Figure 22(b) is submerged by the noise. The contrast results indicate that the proposed optimized continuous complex Morlet wavelet envelope demodulation method can effectively extract the fault characteristics than the Hilbert envelope demodulation method.

VI. CONCLUSION

Aiming at the problem of accurate fault location of the mechanical transmission system of shearer ranging arm, the gear faults are diagnosed by vibration detection method. The combination method of optimized continuous complex Morlet wavelet envelope demodulation spectrum analysis and spectrum analysis is proposed to apply to the accurate gear fault location of the mechanical transmission system of shearer ranging arm. In the algorithm, the optimal center frequency and bandwidth of the Morlet wavelet can be obtained by a wavelet Shannon entropy and the optimal scale factor can be accurately determined by spectrum contrast analysis of vibration signals in normal and fault state.

In order to verify the effect of center frequency and bandwidth on a time-frequency resolution, the simulation signals of fault shock are used. The results indicate that the bandwidth and center frequency optimized by wavelet Shannon entropy can obtain the best time and frequency resolution.

In order to verify the proposed accurate gear fault location method, the vibration signals of MG1480 and MG1660 shearer ranging arm are used to experimental verification. The experiment results indicate that the proposed method can achieve accurate gear fault location of shearer ranging arm. In order to detect the fault of the low-speed shaft and the high-speed shaft of the shearer ranging arm, it is necessary to at least arrange the sensors at the idler and roller shaft. By the contrast of the optimized complex Morlet wavelet envelope demodulation spectrum and the Hilbert envelope spectrum, the results indicate that the proposed optimized complex Morlet wavelet envelope demodulation method can better highlight the fault characteristics than the Hilber envelope demodulation method.

In the future, we will study the fault location method of the mechanical transmission system with variable speed and loads based on this research.

REFERENCES

[1] Q. Li, T. Zhao, L. Zhang, W. Sun, and X. Zhao, "Ferrography wear particles image recognition based on extreme learning machine," *J. Elect. Comput. Eng.*, vol. 2017, pp. 1–6, Jan. 2017.

[2] D. Astolfi, L. Scappaticci, and L. Terzi, "Fault diagnosis of wind turbine gearboxes through temperature and vibration data," *Int. J. Renew. Energy Res.*, vol. 7, no. 2, pp. 965–976, 2017.

[3] W. Wen, X. R. Gao, and W. Cheng, "Planetary gearbox fault diagnosis using envelope manifold demodulation," *Shock Vibrat.*, vol. 7, pp. 965–976, Jan. 2016, Art. no. 3952325.

[4] Z. Li, Y. Jiang, C. Hu, and Z. Peng, "Recent progress on decoupling diagnosis of hybrid failures in gear transmission systems using vibration sensor signal: A review," *Measurement*, vol. 90, pp. 4–19, Aug. 2016.

[5] R. Liu, B. Yang, E. Zio, and X. Chen, "Artificial intelligence for fault diagnosis of rotating machinery: A review," *Mech. Syst. Signal Process.*, vol. 108, pp. 33–47, Aug. 2018.

[6] Z. Wang, Q. Zhang, J. Xiong, M. Xiao, G. Sun, and J. He, "Fault diagnosis of a rolling bearing using wavelet packet denoising and random forests," *IEEE Sensors J.*, vol. 17, no. 17, pp. 5581–5588, Sep. 2017.

[7] D. Zhao, T. Wang, and F. Chu, "Deep convolutional neural network based planet bearing fault classification," *Comput. Ind.*, vol. 107, pp. 59–66, May 2019.

[8] C. Shanshan, "Time domain analysis technology used in diagnosis of machinery equipment fault," (in Chinese), *J. Mech. Transmiss.*, vol. 31, no. 3, pp. 79–85, 2007.

[9] Z. Qiao and Z. Pan, "SVD principle analysis and fault diagnosis for bearings based on the correlation coefficient," *Meas. Sci. Technol.*, vol. 26, pp. 1–15, Jul. 2015.

[10] J. Antoni, "Fast computation of the kurtogram for the detection of transient faults," *Mech. Syst. Signal Process.*, vol. 21, no. 1, pp. 108–124, Jan. 2007.

[11] M. Firla, Z.-Y. Li, N. Martin, C. Pachaud, and T. Barszcz, "Automatic characteristic frequency association and all-sideband demodulation for the detection of a bearing fault," *Mech. Syst. Signal Process.*, vol. 80, pp. 335–348, Dec. 2016.
[12] G. He, K. Ding, W. Li, and X. Jiao, "A novel order tracking method for wind turbine planetary gearbox vibration analysis based on discrete spectrum correction technique," *Renew. Energy*, vol. 87, pp. 364–375, Mar. 2016.
[13] S. Fedala, D. Rémond, R. Zegadi, and A. Felkaoui, "Contribution of angular measurements to intelligent gear faults diagnosis," *J. Intell. Manuf.*, vol. 29, no. 5, pp. 1115–1131, Jun. 2018.
[14] C. Wang, H. Li, G. Huang, and J. Ou, "Early fault diagnosis for planetary gearbox based on adaptive parameter optimized VMD and singular kurtosis difference spectrum," *IEEE Access*, vol. 7, pp. 31501–31516, 2019.
[15] B. Pang, G. Tang, T. Tian, and C. Zhou, "Rolling bearing fault diagnosis based on an improved HTT transform," *Sensors*, vol. 18, no. 4, pp. 1–19, 2018.
[16] W. Teng, R. Jiang, X. Ding, Y. Liu, and Z. Ma, "Detection and quantization of bearing fault in direct drive wind turbine via comparative analysis," *Shock Vib.*, vol. 2016, pp. 1–12, Jan. 2016.
[17] N. G. Nikolaou and I. A. Antoniadis, "Demodulation of vibration signals generated by defects in rolling element bearings using complex shifted Morlet wavelets," *Mech. Syst. Signal Process.*, vol. 16, no. 4, pp. 677–694, Jul. 2002.
[18] Z. Wang, Z. Liu, Z. Deng, W. Deng, and X. Jia, "Phase extraction of nonstationary interference signal in frequency scanning interferometry using complex shifted Morlet wavelets," *Opt. Commun.*, vol. 420, pp. 26–33, Aug. 2018.
[19] Q. Yi, X. Jianfeng, and M. Yongfang, "Weak transient fault feature extraction based on an optimized Morlet wavelet and kurtosis," *Meas. Sci. Technol.*, vol. 27, pp. 1–17, Jan. 2016.
[20] Z. Feng, X. Chen, M. Liang, and F. Ma, "Time–frequency demodulation analysis based on iterative generalized demodulation for fault diagnosis of planetary gearbox under nonstationary conditions," *Mech. Syst. Signal Process.*, vol. 62, pp. 54–74, Oct. 2015.
[21] R. Zhang, X. Gu, F. Gu, T. Wang, and A. D. Ball, "Gear wear process monitoring using a sideband estimator based on modulation signal bispectrum," *Appl. Sci.*, vol. 7, pp. 1–10, Mar. 2017.
[22] Z. Feng, H. Ma, and M. J. Zuo, "Spectral negentropy based sidebands and demodulation analysis for planet bearing fault diagnosis," *J. Sound Vib.*, vol. 410, pp. 124–150, Dec. 2017.
[23] M. Heidari, H. Homaei, H. Golestanian, and A. Heidari, "Fault diagnosis of gearboxes using wavelet support vector machine, least square support vector machine and wavelet packet transform," *J. Vibroengineering*, vol. 18, pp. 860–875, Mar. 2016.
[24] J. Zhu, Y. Xue, N. Zhang, Z. Li, Y. Tao, and D. Qiu, "A noise reduction method for ground penetrating radar signal based on wavelet transform and application in tunnel lining," *Iop Conf.*, vol. 61, pp. 12–88, Apr. 2017.

QINGHUA MAO received the B.Sc., M.Sc., and Ph.D. degrees from the Xi'an University of Science and Technology, in 2007, 2010, and 2012, respectively. He is currently an Associate Professor with the School of Mechanical Engineering, Xi'an University of Science and Technology. His main research interests include non-destructive testing, fault diagnosis, intelligent testing, and control of coal mine mechanical equipment.

YONGQIANG ZHANG was born in 1995. He received the B.Sc. degree from the Xi'an University of Science and Technology, in 2018, where he is currently pursuing the master's degree with the School of Mechanical Engineering. His main research interests include intelligent monitoring, diagnosis, and control of equipment.

XUHUI ZHANG (Member, IEEE) received the B.Sc. and M.Sc. degrees from the Xi'an University of Science and Technology, in 1996 and 2002, respectively, and the Ph.D. degree from Xi'an Jiaotong University, in 2009. He is currently a Professor with the School of Mechanical Engineering, Xi'an University of Science and Technology. His main research interests include intelligent detection and control of equipment.

GUANGMING ZHANG received the Ph.D. degree from Xi'an Jiaotong University, in 1999. He worked as a Postdoctoral Fellow with the State Key Laboratory of Acoustics, Nanjing University. In 2001, he was engaged in research work with Uppsala University, Sweden. Since 2003, he has been working with Liverpool John Morris University, U.K. He is currently a Distinguished Professor with the Hundred Talents Program of Shaanxi Province, School of Mechanical Engineering, Xi'an University of Science and Technology He is an Associate Professor of the school. His main research interests include ultrasonic non-destructive testing, ultrasonic signal processing, scanning acoustic microscopy, micro-nano evaluation, reliability testing of semiconductor devices and packaging, life-span monitoring and forecasting of microelectronic devices, and so on.

HONGWEI FAN received the B.Sc. degree from Beihua University, in 2007, the M.Sc. degree from Northwestern Polytechnical University, in 2010, and the Ph.D. degree from Xi'an Jiaotong University, in 2015. He is currently a Lecturer with the School of Mechanical Engineering, Xi'an University of Science and Technology. His main research interests include intelligent monitoring, diagnosis, and control of equipment.

KUNDAYI MUSHAYI was born in 1993. She received the B.Sc. degree from Shenyang Aerospace University, in 2016. She is currently pursuing the master's degree with the School of Mechanical Engineering, Xi'an University of Science and Technology. Her main research interests include robotics control and machine vision.